Electronic Supplementary Material (ESI) for Journal of Materials Chemistry A.

In-Situ Exsolution of Ag from $AgBiS_2$ Nanocrystals Anode Boosting High-Performance Potassium-Ion Batteries

Xiaoru Ren‡, Dongxu Yu‡, Long Yuan, Yaocai Bai, Keke Huang Jinghai Liu, and *Shouhua Feng**

Synthesis of Bi_2S_3 Nanorods

Typically, 1.0 mmol $Bi(NO_3)_3$ was loaded into a 100 mL three-neck flask fitted with a reflux condenser containing 1 mL OAm, 1 mL OA and 8mL ODE. The mixture was heated to 115 ^{O}C purifying alternatively in vacuum and argon atmosphere for three times to eliminate adventitious water and dissolved oxygen. Afterwards, the system was heated up to the transition temperature of 170 ^{O}C and followed by injection 3 mL N,N'-diphenylthiourea/diphenyl ether solution at the dissolving temperature of 145 ^{O}C via syringe with the color of the solution instantly turned black. The following step are the same as the synthesis process of $AgBiS_2$ NCs.

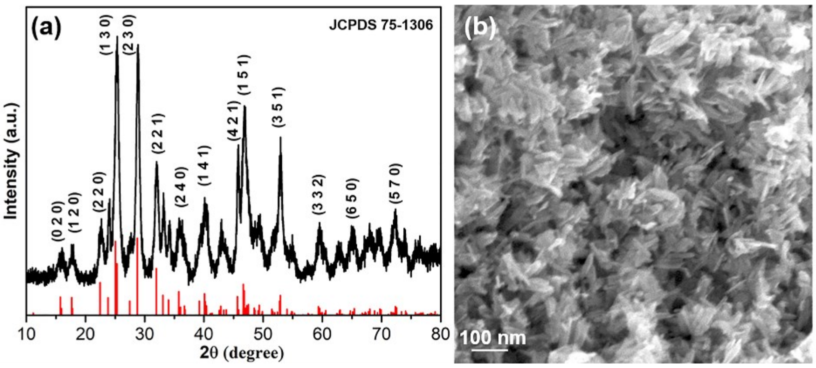

Figure S1. (a, b) XRD pattern and SEM image of Bi_2S_3 NCs.

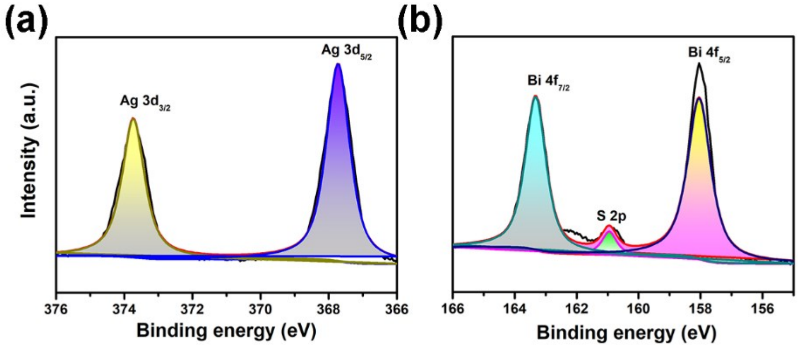

Figure S2. (a, b) XPS spectra of Ag, Bi and S.

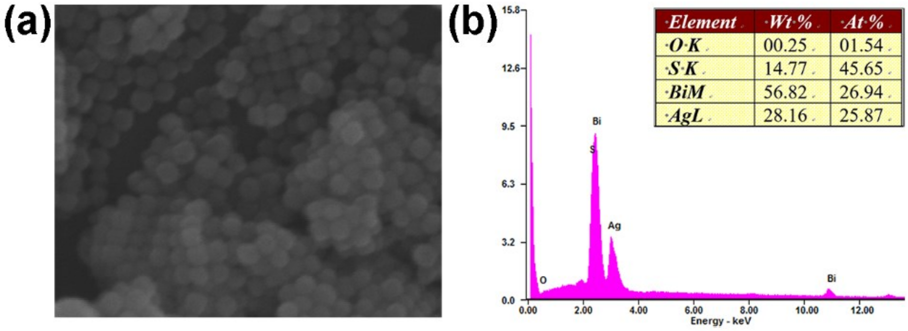

Element	Wt %	At %
O K	00.25	01.54
S K	14.77	45.65
BiM	56.82	26.94
AgL	28.16	25.87

Figure S3. (a, b) The SEM image EDX spectrum of $AgBiS_2$ NCs.

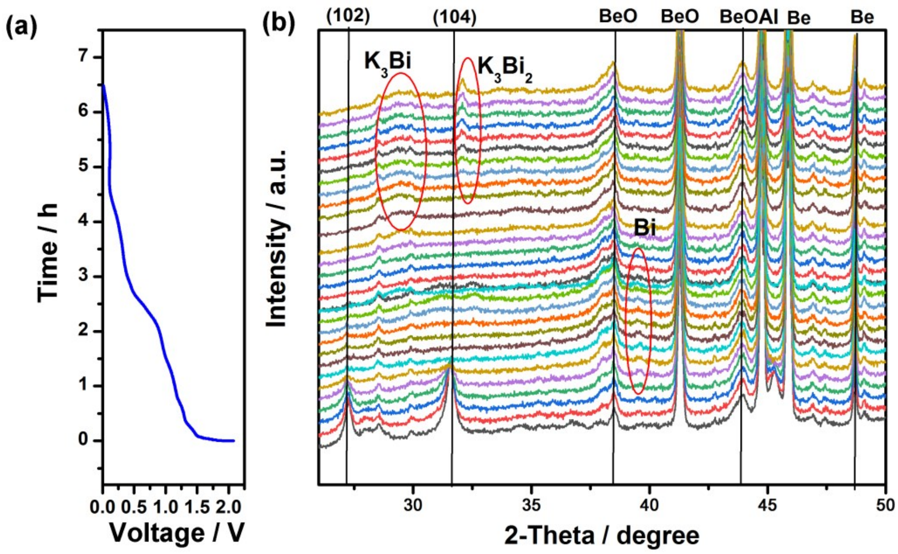

Figure S4. (a) The 1st discharge profile of $AgBiS_2$ at a current density of 0.5 A g^{-1} between 0.01 and 3 V. (b) The voltage profile against *in-situ* XRD patterns in the selected 2-theta regions.

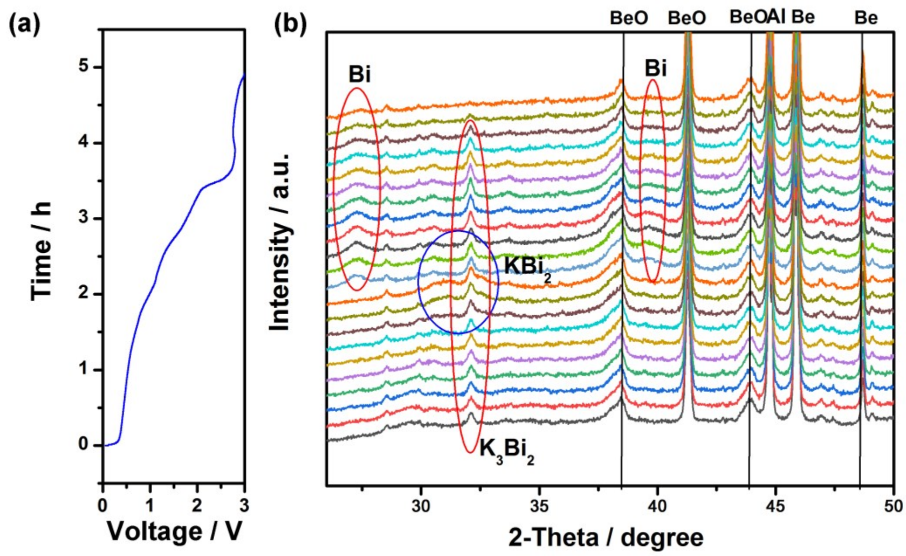

Figure S5. (a) The 1st charge profile of $AgBiS_2$ at a current density of 0.5 A g^{-1} between 0.01 and 3 V. (b) The voltage profile against *in-situ* XRD patterns in the selected 2-theta regions.

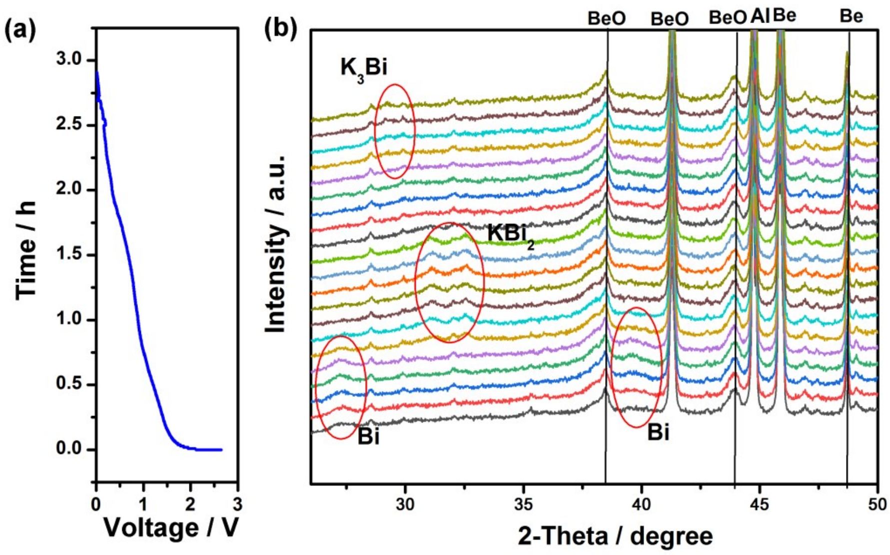

Figure S6. (a) The 2nd discharge profile of $AgBiS_2$ at a current density of 0.5 A g^{-1} between 0.01 and 3 V. (b) The voltage profile against *in-situ* XRD patterns in the selected 2-theta regions.

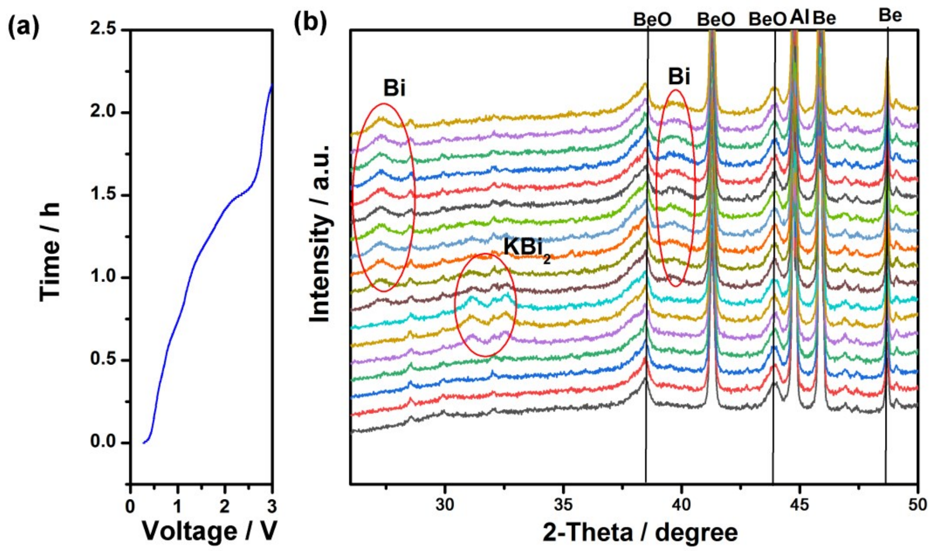

Figure S7. (a) The 2nd charge profile of $AgBiS_2$ at a current density of 0.5 A g^{-1} between 0.01 and 3 V. (b) The voltage profile against *in-situ* XRD patterns in the selected 2-theta regions.

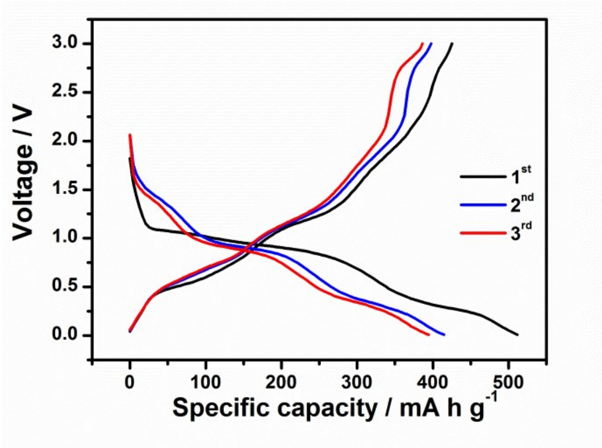

Figure S8. Galvanostatic discharge-charge curves of $AgBiS_2$ nanorods at 0.5 A g^{-1} using Al foil as current collector

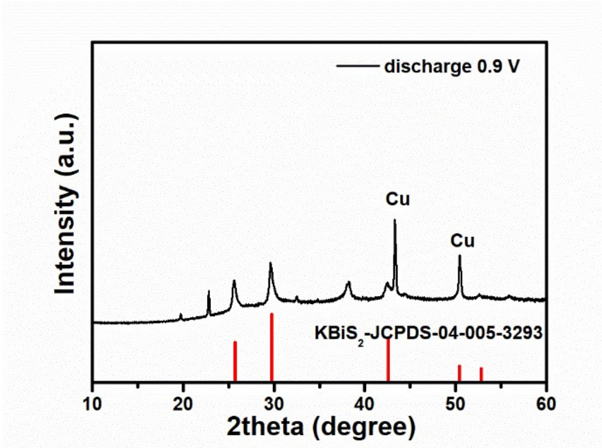

Figure S9. (a) the XRD pattern of $KBiS_2$.

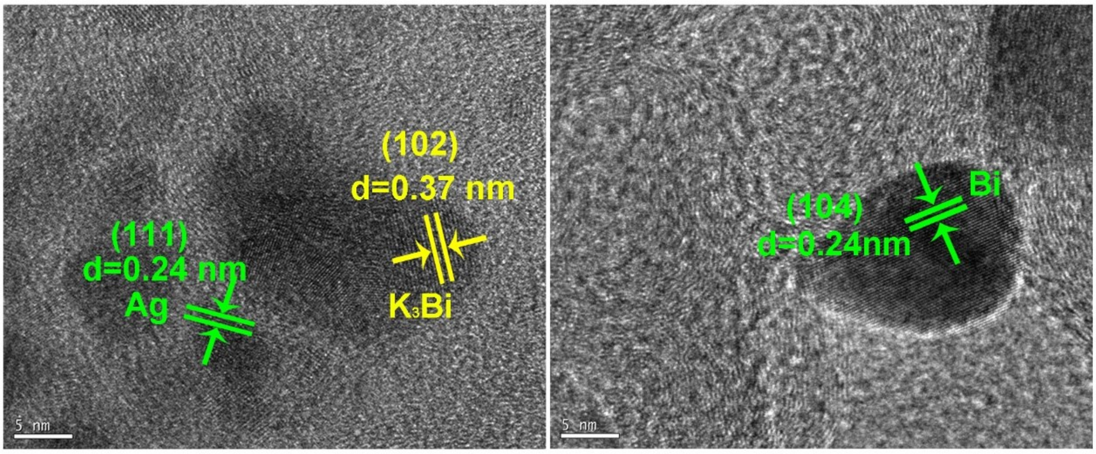

Figure S10 (a, b). HRTEM images of $AgBiS_2$ electrode after being discharged to 0.01 V and charged to 3.0 V.

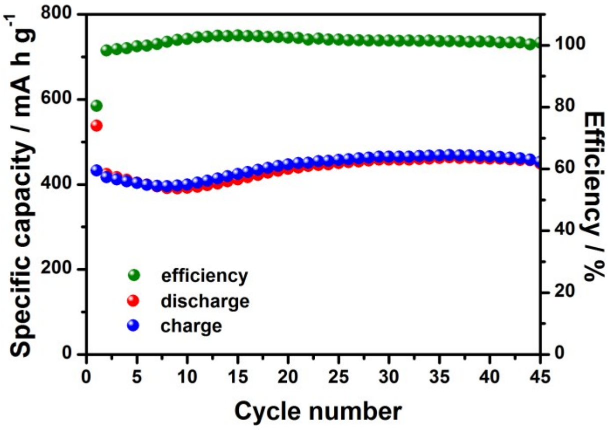

Figure S11. Cycling performance of $AgBiS_2$ nano-octahedrons at 0.5 A g^{-1}.

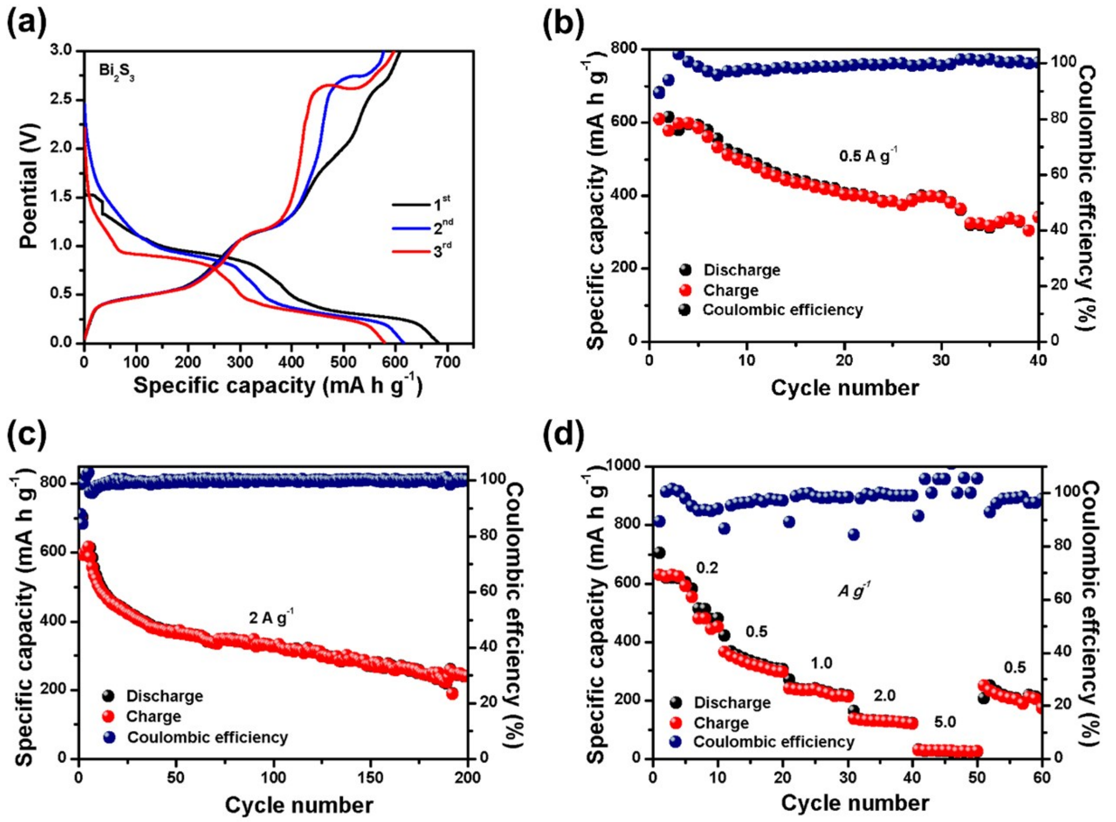

Figure S12. (a) the GCD curves of the Bi_2S_3; (b) the cycling performance at the current rate of 0.5 A g^{-1}; (c) the cycling performance at the current rate of 2 A g^{-1}; (d) the rate performance of Bi_2S_3 at various current rates.

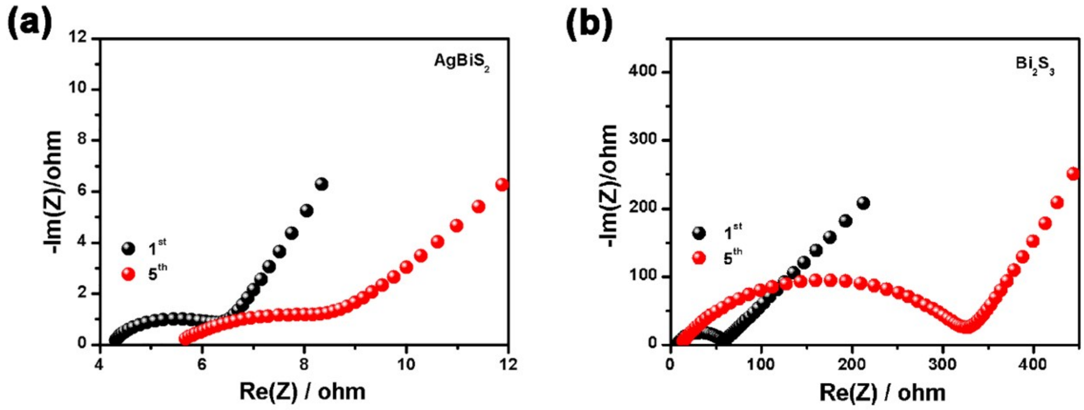

Figure S13. The EIS of different cycles (a) $AgBiS_2$; (b) Bi_2S_3.

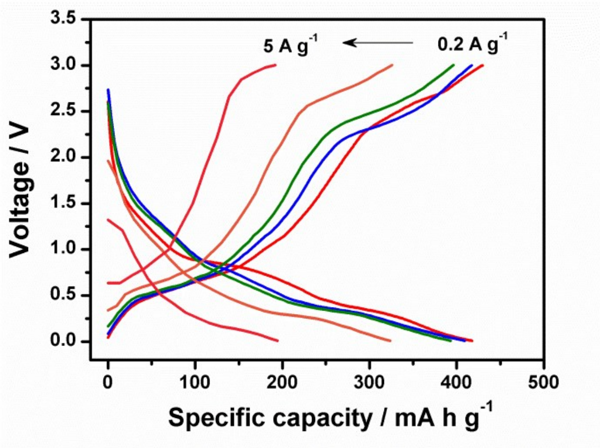

Figure S14. Galvanostatic discharge-charge curves of $AgBiS_2$ nanocubes at various current densities from 0.2 to 5 A g^{-1}.

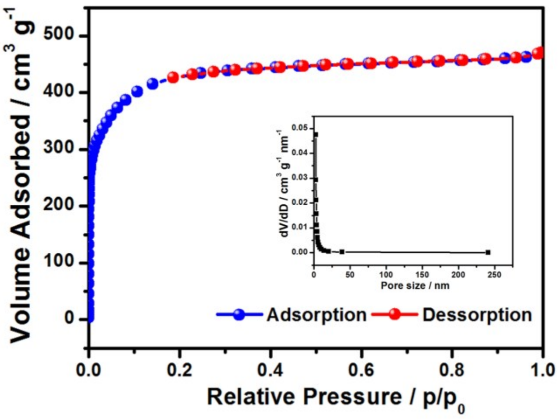

Figure S15. N_2 adsorption-desorption isotherms of AC

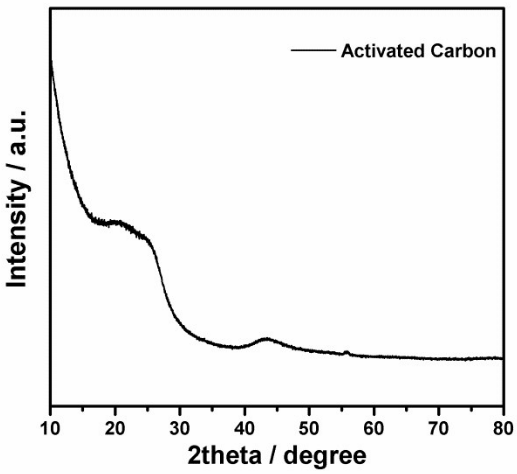

Figure S16. XRD pattern of Activated Carbon (AC)

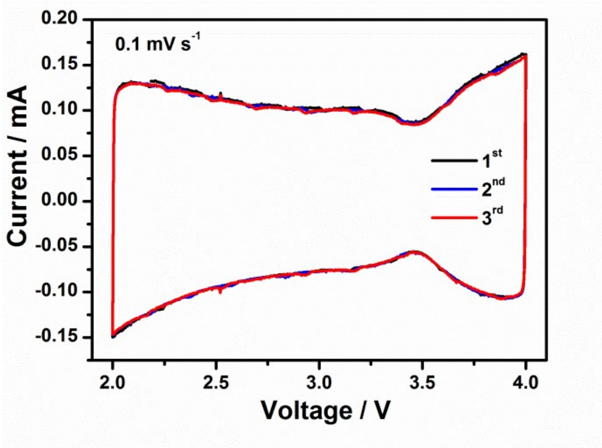

Figure S17. CV curves of AC at 0.1 mV/s

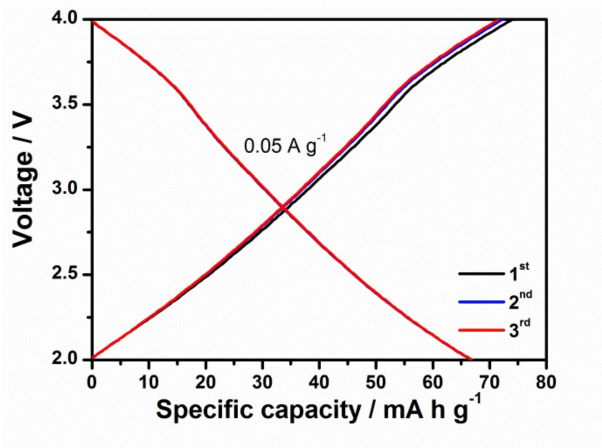

Figure S18. Charge-discharge profiles of AC at 0.05 A/g between 2.0 -4.0 V;

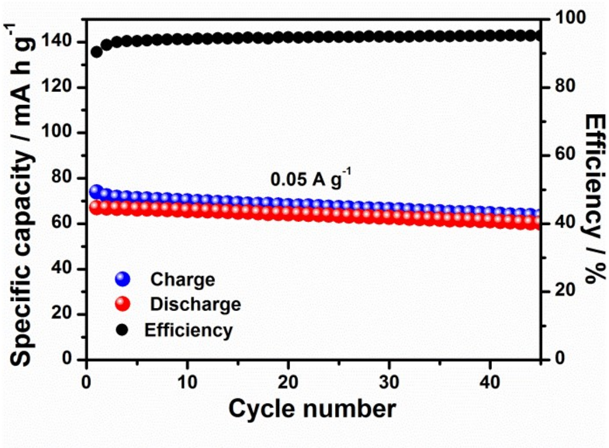

Figure S19. Cycling performance of AC at 0.05 A/g

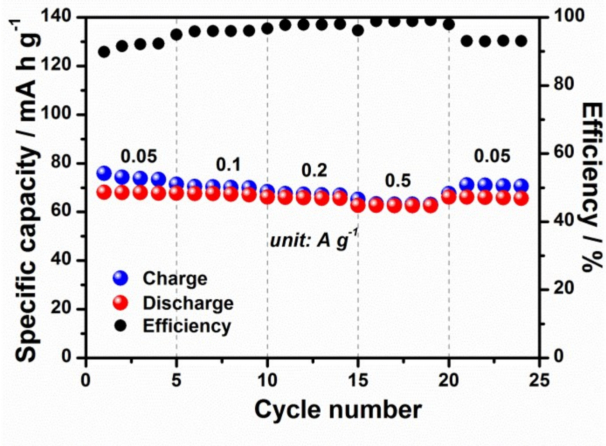

Figure S20. Rate capacity of AC

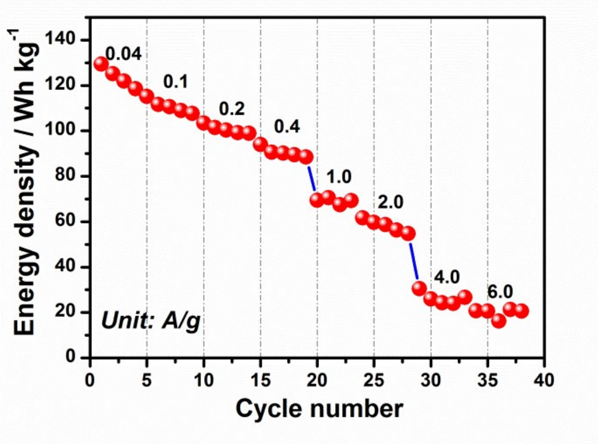

Figure S21. Rate performance of AC//$AgBiS_2$ hybrid capacitor at various current densities

Table S1. Comparison of energy density for various KIHCs

Active Material	Energy Density (Wh kg^{-1})	Power Density (W kg^{-1})	Year
(N, S)-3DHPC//AC	130.6	210	2020
CNSs//AC	149.0	210	2019
NCHS//WS_2@NCNs	103.4	235	2019
Bi//$K_{0.72}Fe[Fe(CN)_6]$	108.1	566	2018
$K_2Ti_6O_{13}$//NGC	58.2	~160	2018
$Ca_{0.5}Ti_2(PO_4)_3$@C//AC	80	32	2018
K_2TP//AC	46	101	2018
$AgBiS_2$//AC	118.5	98.8	this work